



Subsurface and Bulk Residual Stress Analysis of S235JRC + C Steel TIG Weld by Diffraction and Magnetic Stray Field Measurements

T. Mishurova¹ · R. Stegemann² · V. Lyamkin³ · S. Cabeza⁴ · S. Evsevlev¹ · M. Pelkner¹ · G. Bruno^{1,5}

Received: 9 July 2021 / Accepted: 22 March 2022
© The Author(s) 2022

Abstract

Background Due to physical coupling between mechanical stress and magnetization in ferromagnetic materials, it is assumed in the literature that the distribution of the magnetic stray field corresponds to the internal (residual) stress of the specimen. The correlation is, however, not trivial, since the magnetic stray field is also influenced by the microstructure and the geometry of component. The understanding of the correlation between residual stress and magnetic stray field could help to evaluate the integrity of welded components.

Objective This study aims at understanding the possible correlation of subsurface and bulk residual stress with magnetic stray field in a low carbon steel weld.

Methods The residual stress was determined by synchrotron X-ray diffraction (SXR, subsurface region) and by neutron diffraction (ND, bulk region). SXR possesses a higher spatial resolution than ND. Magnetic stray fields were mapped by utilizing high-spatial-resolution giant magneto resistance (GMR) sensors.

Results The subsurface residual stress overall correlates better with the magnetic stray field distribution than the bulk stress. This correlation is especially visible in the regions outside the heat affected zone, where the influence of the microstructural features is less pronounced but steep residual stress gradients are present.

Conclusions It was demonstrated that the localized stray field sources without any obvious microstructural variations are associated with steep stress gradients. The good correlation between subsurface residual stress and magnetic signal indicates that the source of the magnetic stray fields is to be found in the range of the penetration depth of the SXR measurements.

Keywords Residual stress · Magnetic stray field · Synchrotron X-ray diffraction · Neutron diffraction · TIG-welding

Introduction

Mechanical stresses can change the magnetic hysteresis of ferromagnetic materials. The connection between mechanical and electromagnetic phenomena is known as the magneto-mechanical effect [1, 2]. It is important to note that the actual *intrinsic material property* of ferromagnetic materials, the anisotropic magnetization M [1] is temperature-dependent and hardly affected by mechanical loads. Specimens in high external magnetic excitation fields H_{ext} reach a saturation magnetization M_s . The induction B and the field strength H are structural quantities of a specimen and depend not only on the microstructure and the properties of its constituent materials, but also significantly on the shape of the specimen [3].

Consequently, the mechanical stress does not alter the magnetic moment itself but causes a change of the preferential directions of M in a specimen. This is observed by

✉ T. Mishurova
tatiana.mishurova@bam.de

¹ Bundesanstalt Für Materialforschung Und -Prüfung (BAM),
Unter den Eichen 87, 12205 Berlin, Germany

² Umlaut Systems GmbH, Am Hauptgüterbahnhof 25,
38126 Braunschweig, Germany

³ Chair of NDT and Quality Assurance (LZfPQ), Saarland
University, Campus Dudweiler, 66125 Saarbrücken,
Germany

⁴ Institut Laue-Langevin, 71 avenue des Martyrs CS 20156,
38042 Grenoble, Cedex 9, France

⁵ University of Potsdam, Karl-Liebknecht-Strasse 24/25,
14476 Potsdam-Golm, Germany



comparing the magnetic hysteresis in the so-called easy and hard directions. The difference of the magnetic polarization (hysteresis loops) between two true elastic tensile stress states is small [1, 4–6]. In contrast, the difference between the magnetic hysteresis of specimens subjected to tensile and to compressive stress states [4–6] (different deviatoric stress states) is more apparent [7–12] since the magnetic anisotropy is enhanced [13].

The conventional non-destructive magnetic inspection techniques [14, 15] utilize homogenization and polarization *vs.* saturation magnetization for crack detection. In fact, cracks cause a local maximum of the so-called magnetic stray fields (SFs) [16–19]. SFs are demagnetization fields outside the specimen under investigation [3]. In contrast, the permeability differences due to mechanical stress and other microstructural characteristics (*e.g.* grain size, phases) are particularly noticeable in so-called weak (internal) magnetic fields within the coercivity ($\pm H_C$) limits [1, 2, 6]. Field strengths higher than H_C will enforce a homogenization, *i.e.* polarization towards saturation M_s , suppressing the local magnetization difference as a source of SFs.

If two specimens of different magnetically sensitive materials are joint, a localized SF will emerge at their interface [16, 20]. However, such SFs are denoted as “weak” compared to magnetic crack detection, since the difference between the (bulk average) magnetization of two unsaturated ferromagnetic materials is usually small [16–19].

Such “weak” fields can nowadays be measured utilizing small, point-like, magnetic field sensors such as AMRs (anisotropic magnetoresistors) [21–23]. In fact, while the magnetization of a whole specimen may appear weak on average, the single magnetic domains are saturated [13, 24].

Due to heating and rapid cooling rates during welding, non-uniform contraction and expansion occur, resulting in a distinct residual stress (RS) profile [25–27]. RS is a well-known issue affecting the mechanical performance and the structural integrity of welded components (the literature on the subject is enormous, see [28–31] as examples). Such RS profiles with large stress gradients make welds the perfect case studies for the present research: we aimed to correlate the RS with magnetic SF measurement in engineering materials and components. In fact, in our previous studies [32, 33], we showed that the magnetic SFs are causally linked to the microstructure in the fusion zone (FZ), the heat affected zone (HAZ), and the surrounding (parent) material. These zones could be distinguished by utilizing high-spatial-resolution giant magneto resistance (GMR) sensors. The SF leak out of the surface (indicating a local difference in magnetization) is represented by a vector pointing inwards, analogously to the typical SF signal of a crack in magnetic flux leakage testing [15–19]. Thus, the measurements of the magnetic SF by GMR sensors is called GMR-SF in the remainder of the text.

Besides the SF being causally related to microstructural changes in welds [33], the most pronounced SF signals were found far from the weld and HAZ, in areas where no obvious (*i.e.* visible in an optical microscope) microstructural changes occurred. Yet in such regions, a steep change of RS from compressive to tensile was found by Neutron Diffraction, ND, experiments. The shape of the RS and SF profiles across the weld seam and the position of their the maxima correlated well but did not perfectly match. In [32, 33] we explained these differences invoking the different regions probed by each of the two methods: the ND method usually probes the stresses in the bulk whereas the SF could mainly be influenced by near-surface stresses. To address this issue, synchrotron X-Ray Diffraction (SXR) is proposed in this study. SXR allows determining RS in the subsurface regions of a specimen and, thus, probes nearly the same regions as GMR-SF technique. In fact, this study demonstrates the correlation between well-established (diffraction-based) techniques, SXR and ND, for RS analysis and observations by magnetic GMR-SF measurements.

Material and Methods

Material Processing and Characterization

The investigated test sample was a cold-drawn steel plate made of S235JRC + C, a commercial ferromagnetic low-carbon structural steel (material no. 1.0120). The sample was a plate with sizes 250 mm \times 100 mm \times 4.8 mm (length \times width \times thickness); both top and bottom surfaces of the plate were ground after welding. After demagnetization, the plate was welded on its top in the middle (see Fig. 1) using tungsten inert gas (TIG) welding without filler. The absence of filler would prevent any change of the material composition across the weld. Therefore, only the RS and the microstructure (grain size and morphology) of the different zones of the weld would contribute to the magnetic stray fields because of their influences on the magnetic properties. The speed of the welding electrode was 200 mm/min and the applied current was 200 A.

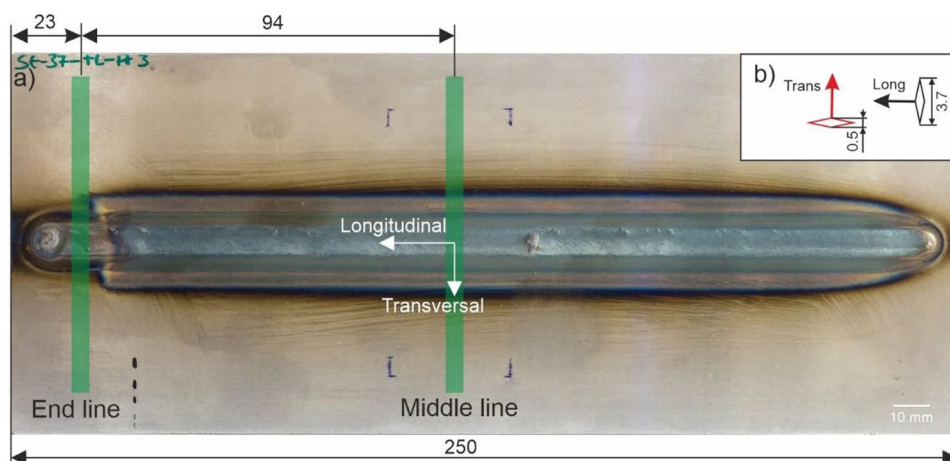
For optical microscopy, a sister plate (a welded plate produced with the same parameters as the sample under investigation) was sliced transversal to the weld. The surface was then ground, polished, and etched using Nital.

Magnetic Field Measurements

To map the magnetic SFs at the surface of a component, appropriate magnetic field sensors are needed. Their sensitive elements must be small for high-resolution measurements. In addition, the sensitive elements must be placed



Fig. 1 a) A photograph of the plate, showing the position of SXR (and ND) measurement lines (green) and b) the scheme of the gauge volumes used in SXR measurement (projected to LT plane). Note: the shape of the gauge volume is simplified, for details see [35]. The dimensions are given in mm



close to the surface to increase the signal-to-noise ratio (SNR). The deployed GMR sensor “12A” (designed by BAM, produced by Sensitec GmbH, Wetzlar, Germany) was a gradiometer measuring a difference of the normal field component ΔH_N of the magnetic flux leaking out of the surface. One element of the gradiometer was placed at the edge of a chip. The second element was 250 μm above the first element. The nominal size of each sensing element was $25 \times 35 \mu\text{m}^2$ [23]. The sensitivity of the sensors is 3 mV/V (kA/m). GMR sensors were operated using a supply voltage of 5 V provided by a low-noise DC power source.

The distance between sensor and surface under test, the so-called lift-off, should be as small as possible; therefore, we positioned the sensor around 100 μm above the specimen. Reduced lift-off results in an enhanced SNR since stray fields are localized at the surface. To further enhance the SNR, we scanned the specimens with six different sensors of the GMR array, pre-amplified signal of the collected data, and averaged the GMR-SF profiles over all 6 collected data sets. The measurement points had a pitch of 16 μm in the direction transversal to the weld and 35 μm in the direction along the weld. The test specimen was moved beneath the fixed sensor with a velocity of 40 mm/s.

Uncertainties in GMR-SF scans can be split to positioning and sensor response errors. The most important positioning error is the variation in the lift-off, since the GMR-SF varies significantly with the distance from the surface. However, for a single scan this distance remains constant; this means that this type of error can be neglected for the comparison of features within a single image/scan. To make sure no significant tilt of the plate was present, the lift-off was (visually) confirmed prior to the scanning to be identical in all four corners of the scanning area. Planar or XY positioning error can be also neglected, since the position repeatability of the linear actuators used ($< 1 \mu\text{m}$) significantly exceeds the maximum lateral resolution of the GMR sensor ($\sim 50 \mu\text{m}$). Errors originating from the sensor and data acquisition equipment

may also arise, but the above-mentioned average of six different GMR pairs strongly reduced such errors. Also, scans were performed at least twice on each sample to make sure no spontaneous external magnetic field was present during the measurements. Further experimental details and further information can be found in [32, 33].

Residual Stress Determination

For the RS characterization in the subsurface region of the welded plate, the SXR experiment was performed at the beamline EDDI (synchrotron BESSY II, HZB, Germany) [34]. This beamline was operated in energy dispersive mode and provided a white beam with an energy range of about 10 keV – 150 keV. A liquid-nitrogen cooled Ge solid-state detector from Canberra (model GL0110) was used. The measurements using the $\sin^2\psi$ method were conducted in reflection-mode with the specimens mounted on a Eulerian cradle. This approach assumes biaxial stress state at the surface (*i.e.*, the RS component normal to the surface is close to zero [35]).

The full weld sample with the size of 250 mm \times 100 mm \times 4.8 mm (as shown in Fig. 1) was mounted on the beamline. Two lines at the top surface of the plate were scanned (middle line and end line, see Fig. 1(a)), also the middle line at the bottom surface of the plate was measured. The measurement points had a distance of 1 mm between each other. At each point two directions were measured: transversal (T) and longitudinal (L). Figure 1(b) shows the projection of the gauge volume (GV) onto the LT plane for each of the plate orientations. The prismatic GV was defined by the intersection of the incoming beam (the vertical and horizontal opening were 0.5 mm) and the diffracted beam (the secondary slits vertical opening was 30 μm). The effective GV had a largest diagonal of 3.7 mm. Therefore, for the longitudinal stress component the GV's of neighboring measurement points were overlapping, while for transversal they were separated (see schematic in

Fig. 2 Optical micrograph of the cross-section of the sister sample with the schematic of used GV in SXR and ND measurement (for transversal stress component), as well as with the indication of the geometry of the GMR-SF experiments

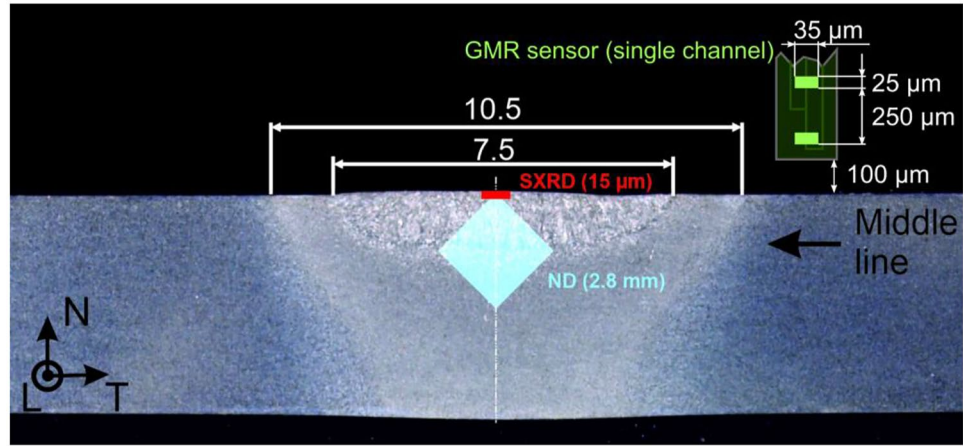


Fig. 1(b)). The Fe-211 ferrite peak was chosen for the SXR analysis. This reflection was the same used in ND experiments for analysis of *bulk* RS; the penetration depth of X-rays was around 15 μm (while for neutrons, points were taken up to the mid-thickness of the welded plate).

Assuming vanishing shear stresses, the fundamental equations of X-ray stress analysis for the T strain (azimuth $\varphi = 0^\circ$, strain $\varepsilon_{0,\psi}$ is the) and L strain component ($\varphi = 90^\circ$ strain $\varepsilon_{90,\psi}$) read as [36]

$$\varepsilon_{0,\psi} = \frac{1}{2} s_2 \cdot \sigma_T \cdot \sin^2 \psi + s_1 \cdot (\sigma_T + \sigma_L) \quad (1)$$

$$\varepsilon_{90,\psi} = \frac{1}{2} s_2 \cdot \sigma_L \cdot \sin^2 \psi + s_1 \cdot (\sigma_L + \sigma_T) \quad (2)$$

where σ_T and σ_L are the transversal and longitudinal RS, and s_1 and $\frac{1}{2}s_2$ are the so-called diffraction elastic constants (DEC) [37]. DEC were calculated by Eshelby-Kröner model [38] for Fe-211: $s_1 = -1.27 \times 10^{-6} \text{ MPa}^{-1}$ and $\frac{1}{2}s_2 = 5.8 \times 10^{-6} \text{ MPa}^{-6}$. The error bars for RS were calculated using first the uncertainty in the determination of the diffraction peak position (peaks are fitted with a Pseudo-Voigt function), and then propagated to the uncertainty in the least-square fitting of the ν vs $\sin^2 \psi$ plots from equations (1) and (2). (see example in [39]).

The equivalent von Mises stresses were calculated according to:

$$\sigma_{vM} = \sqrt{\sigma_T^2 - \sigma_T \sigma_L + \sigma_L^2} \quad (3)$$

Finally, the Pearson correlation coefficient (r) was calculated to estimate the correlation between RS (σ) and GMRSF signal (ΔH) as

$$r = \frac{\sum (\sigma_i - \bar{\sigma}) (\Delta H_i - \overline{\Delta H})}{\sqrt{\sum (\sigma_i - \bar{\sigma})^2 \cdot \sum (\Delta H_i - \overline{\Delta H})^2}} \quad (4)$$

where t is the position along the measurement lines (*i.e.* in the T direction).

In this work, the SXR results are compared with ND results, published previously. The experimental details for the ND experiment can be found in [32, 33].

Results

The weld (or else fusion zone, FZ) and heat affected zone (HAZ) can be identified in brighter contrast within the middle of the optical micrograph of the sample cross-section (Fig. 2); the parent material at both edges has a darker contrast. The cross-section is taken perpendicular to the weld seam, at the middle line (see Fig. 1). The schematic of the GV probed by SXR and ND as well as the schematic of GMR sensor placed above the sample surface are shown in Fig. 2. ND probes the bulk of the plate (to a depth of around 2.8 mm from the surface), and thus averages the stresses in the whole thickness of the FZ and part of HAZ (the FZ is about 1.8 mm thick). In contrast, SXR probes a subsurface region of around 15 μm depth and differentiates regions belonging to the HAZ or to the FZ. The penetration depth of GMR-SF measurements is difficult to quantify. However, since it is a subsurface technique, we assume the penetration to be comparable with that of SXR measurements.

Figure 3(a), (b) shows the results of the GMR-SF measurements on the top surface of the plate. In both the 2D map and in the line scan the different regions across the weld (HAZ and FZ) can be distinguished. The microstructure of the different regions is summarized in Fig. 3(c). The parent material shows a ferritic-pearlitic microstructure with an average grain size of around 18 μm . It also shows larger grains compared to the HAZ, due to recrystallization (Fig. 3(c)). Also, in the case of the HAZ, a bimodal distribution of coarse and fine recrystallized grains can be observed.



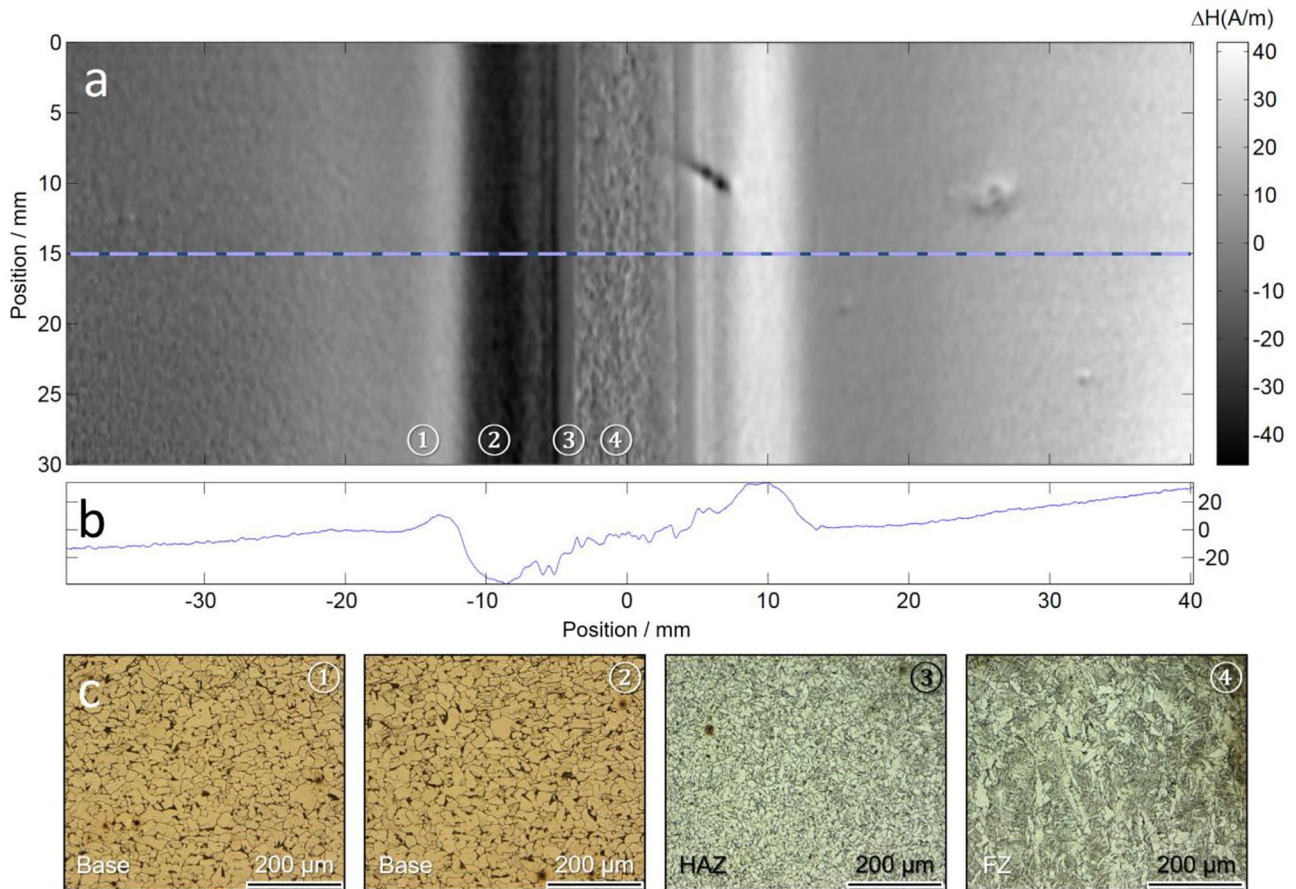


Fig. 3 The Low Carbon Steel S235JRC+C welded plate: **a**) 2D GMR-SF (ΔH_N) map; **b**) GMR-SF profile along the dashed line in (a); **c**) micrographs of a cross-sections of a sister sample: ① & ② parent material; ③ heat affected zone (HAZ), ④ fusion zone (FZ); for further details see [33]

The FZ presents a bainitic Widmanstätten microstructure with acicular ferrite (Fig. 3(c), region 4).

Figure 4 summarizes the RS profiles at the subsurface (SXR) and in the bulk (ND), compared with the magnetic GMR-SF measurements at the top surface of the plate (where the weld seam is located). The pink line represents the weld region (FZ) and the green line represents the HAZ. The maximum stress values are larger at the subsurface than in the bulk. This behavior can also be related to the microstructural gradient along the thickness (as shown in Figs. 2, 3). It has been reported that stresses along a TIG-weld thickness, start with maximum tensile stresses at the surface and are balanced by compressive stress in the middle [40]. Although the maximum stress difference between ND and SXR for σ_L reaches around 100 MPa, the location of the maxima is almost the same for both probes (and located at each side of the weld pool, around 7 mm from the center). The stress peaks are sharper for the subsurface than for the bulk RS profiles (Fig. 4(a), (c)). This is related to the GV size of each technique: neutrons average the signal over a much larger region

than X-rays; thus, the ND RS profile is smoother. Interestingly, for the middle line the width at the half-height of the σ_L peaks as determined by SXR is similar to the width of the GMR-SF peaks (around 3.5 mm). For the end line, the amplitude of the maximum GMR-SF signal decreases (compare the H scales in Fig. 4(a) and (c)), and the distribution becomes narrower. This is also observable for the stress maxima (especially σ_L) measured by SXR. One can notice that RS profiles are shifted with respect to the weld for the end line: the maxima of stress are not symmetric with respect to the center of the weld (the difference is around 1 mm, Fig. 4(a), (c)). This asymmetry is even opposite for ND and SXR data sets. This maybe caused by a slight misalignment of the plate during set-up of the diffraction measurements. Obviously, the irregular geometry of the weld, *i.e.* a slight change in geometry and dimension of the weld seam at the end of welding process (see Fig. 1) may also play a role.

The σ_T component (Fig. 4(b), (d)) presents more variations in the HAZ and FZ for the subsurface profile than for the bulk one. The bulk stresses (ND) stay almost con-

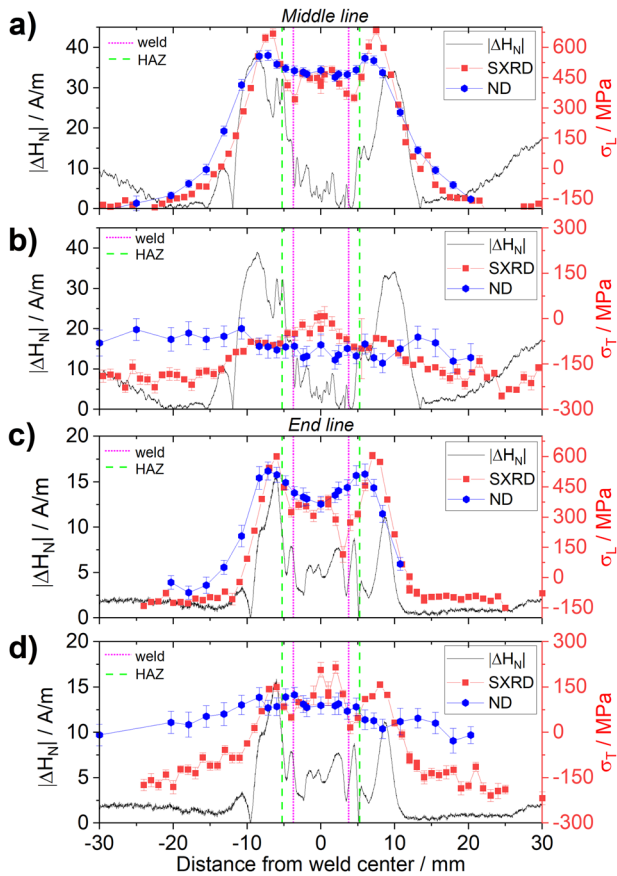


Fig. 4 Comparison of GMR-SF $|\Delta H_N|$ with surface (SXR) and bulk (ND) RS at the top surface for the middle line **a)** σ_L , **b)** σ_T ; and for the end line **c)** σ_L , **d)** σ_T

stant along the scanned lines. As mentioned above, SXR mapping has a higher spatial resolution along the transversal direction compared to ND (see Figs. 1, 2). Therefore, the maxima of RS in the middle of the weld can be better distinguished by means of SXR for the transversal component than in the ND data (Fig. 4(b)). Additionally, for the end line the two maxima (up to 150 MPa) coincide with the positions of the $|\Delta H_N|$ maxima. In the FZ some oscillations of $|\Delta H_N|$ are visible. They are most probably caused by the microstructural changes from the FZ to the HAZ and the parent material (see Fig. 3). The comparison between the bulk stress profiles and the subsurface ones confirms that the changes in the microstructure strongly affect the stress gradients. Therefore, regions with less clear microstructural changes display smaller stress oscillations. This further confirms that GMR-SF and SXR signals do probe the same features of the microstructure and are affected in the same manner by such features and by the stress state. This also implies that, while difficult to estimate, the penetration depth of the GMR-SF signal well corresponds to that of synchrotron X-rays.

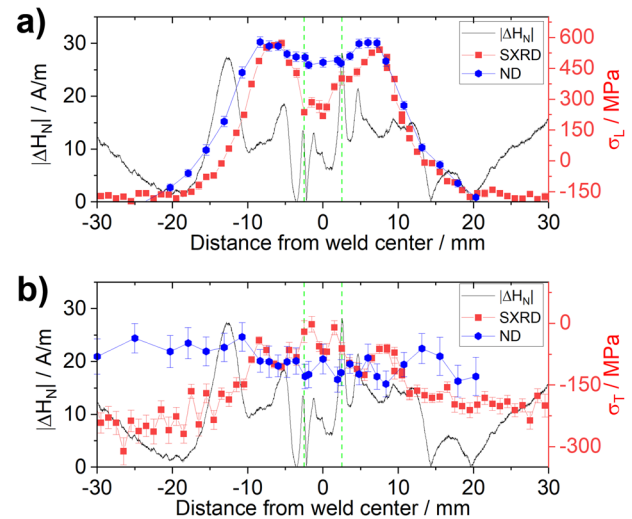


Fig. 5 The comparison of GMR-SF $|\Delta H_N|$ with surface (SXR) and bulk (ND) RS at the bottom surface of the plate, for the middle line: **a)** σ_L , **b)** σ_T

The magnetic GMR-SF measurements along the middle line at the bottom of the plate (Fig. 5) show less pronounced maxima compared to those at the top surface. In fact, they probe only the HAZ at the bottom of the plate. The large peak of the magnetic GMR-SF signal profile still corresponds to the region of steep gradient of the longitudinal RS component (see Fig. 5(a) on the left). As it is visible at the cross section of the sample (see Fig. 2), the bottom of the plate presents no FZ and therefore microstructure, magnetic GMR-SF signal and RS must differ from those at the top surface.

Discussion

In this chapter, only the data regarding the top surface of the plate are discussed. The equivalent von Mises stresses (σ_{VM}) were calculated according to equation (3) for each measured point. They are displayed in Fig. 6. The maxima of the GMR-SF and RS profiles are consistently found in the so-called “strain affected zone” (SAZ) [41, 42], which extends beyond the HAZ, up around to 10 mm on either side of the weld seam. The SAZ is larger than the HAZ optically visible in Fig. 2, as already found elsewhere [30]. In our previous study [33], we showed that no variation of microstructure (grain morphology and size) takes place in the region with maximum $|\Delta H_N|$. As mentioned above, the asymmetry of the SXR stress profile with respect to weld position at the end line is pronounced, so that for further analysis of the correlation between SXR and GMR-SF data, the profile was shifted by +1 mm.



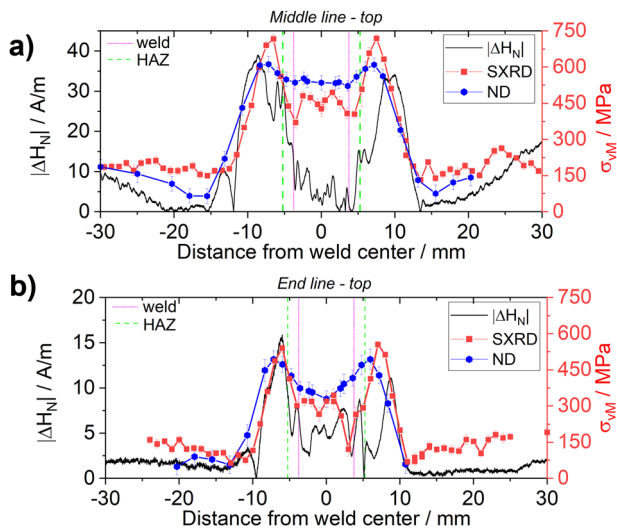


Fig. 6 The comparison of $|\Delta H_N|$ and von Mises stresses σ_{VM} for: **a)** the middle line, **b)** the end line (measurements at the top surface of the plate)

In order to extend the analysis of the correlation between magnetic and diffraction signals beyond the visual comparison available in Figs. 4–6, correlation plots between the magnetic GMR-SF signal and the values of the subsurface σ_L component were built. They are presented in Fig. 7(a), (b), where we separate the analysis of the values in the HAZ and outside it (labelled w/o HAZ). In the HAZ (including the FZ, *i.e.* at the positions $-6 \text{ mm} \geq t \geq 6 \text{ mm}$ along the transverse direction), there seems to be no correlation between the subsurface RS profile (Fig. 7(c), (d)), and the GMR-SF. This implies that the GMR-SF signal variation is heavily influenced by the microstructure in this region [33] (indeed, structural noise appears in the GMR-SF profile - see the blue shaded region in Fig. 7(c), (d)). In contrast, in the SAZ [29,

41–43] –outside the HAZ—an area with high RS values is visible and the correlation with the GMR-SF signal is stronger (Fig. 7(a), (b)). Some points with very high RS (above 600 MPa) display different values of GMR-SF (circled regions in Fig. 7(a), (b)). Such points belong to the transition between the HAZ and the parent material, where the RS profiles have maxima, but the GMR-SF profile is still changing. This may imply that for very high stress values the effect of the microstructure is still large on the GMR-SF signal, and the correlation between GMR-SF and SXR breaks down. The RS presents better correlation inside the HAZ/FZ at the end line compared with the middle line. As an example, it is to be noted that the GMR-SF profile in Fig. 7(d) appears to possess the same distinct dip at around 3 mm from the weld center as the RS determined by SXR. Such dip is not visible in the analogous ND RS profile. Interestingly, for the end line some of the blue points (belonging to the HAZ) do fall on the linear correlation between SXR and GMR-SF signals.

These observations are also confirmed by the correlation coefficients presented in Fig. 8 (calculated according to equation (4)). The correlation between the two stress components and the von Mises stress is increased when separately considering the regions outside the HAZ for both ND and SXR. For the end line, the correlation coefficient between SXR and GMR-SF is much higher compared with that between ND and GMR-SF (Fig. 8(b)). In the case of the middle line, the correlation coefficients of the longitudinal and the von Mises stress are similar. However, for the transversal component a drastic increase of the coefficient is observed for SXR (in the regions excluding the HAZ). This effect is related to the fact that both GMR-SF and SXR probe subsurface regions, and SXR possesses higher spatial resolution than ND for the transversal component. The higher spatial resolution of SXR allows capturing some

Fig. 7 Top row: Longitudinal surface RS from SXR measurements as a function of GMR-SF $|\Delta H_N|$ for: **a)** the middle line and **b)** the end line. Bottom row: $|\Delta H_N|$ and surface RS as a function of position along the weld for: **c)** the middle line, **d)** the end line. Note: the blue and green regions at **c)**, **d)** correspond to the blue and green points in **a)**, **b)**. Circled regions correspond to the points belonging to the transition between the HAZ and the parent material, where high stress values are observed

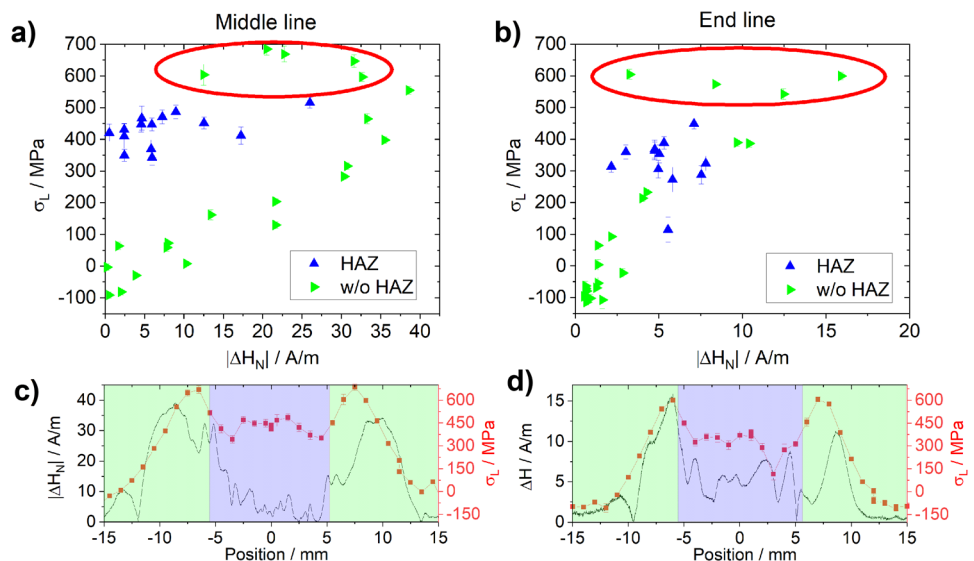
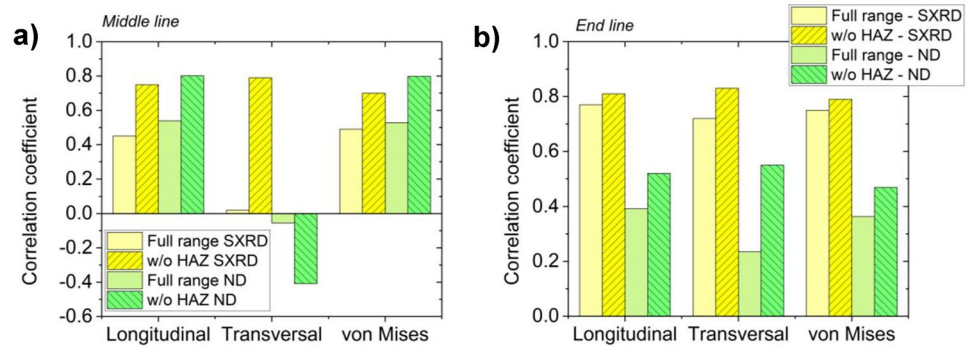


Fig. 8 Correlation coefficient between GMR-SF signal and surface RS determined by SXRD and bulk RS determined by ND for: **a)** the middle line, **b)** the end line



details of the RS profiles that are averaged out in ND data. The different resolution and the fact that ND probes inner regions of the plate, both cause the correlation between ND and GMR-SF to be worse than that between SXRD and GMR-SF (typical values of the coefficient around 0.4–0.6 for ND vs 0.8 for SXRD).

We need to consider that the plate was subjected to a significant magnetic field due to the welding process (magnetic field linked to the welding current), as well as to the magnetic field of the Earth. In the case of passive magnetic stray field measurements, the data should be taken as an integral of the "magnetic history" – *i.e.* the residual magnetic field – in the presence of a magnetic anisotropy caused by microstructure and (residual) stress variations.

On a fundamental level, one cannot expect a bijective correlation between GMR-SF and RS profiles. The comparison of a second rank stress tensor to a near-surface magnetic vector field will entail a loss of information. In addition, the passive magnetic field measurements also depend on the shape of the test object itself. It appears therefore more important to evaluate the effect of spatial stress tensor transitions on magnetic GMR-SF as is to be expected from magneto-mechanical hysteresis measurements. The good correlation between the locations of the RS maxima and the magnetic stray field concentrations could be practically used to evaluate the integrity of welded components. Further research is needed to establish the cause-effect relationship between the RS gradients and the magnetic stray fields in systems with complex multi-axial stress distributions and with varying microstructural and magnetic properties, such as dissimilar welds or additively manufactured components.

Conclusions

The evaluation of the influence of complex residual stress states on magnetic stray field (SF) distributions requires detailed benchmark and correlation of the material microstructure and stress state characterization. In order to do so, the spatial resolution of residual stress analysis by diffraction methods,

microstructural investigations, and GMR-SF measurements need to match within a reasonable tolerance.

Our investigations prove that magnetic stray fields of a S235JRC + C weld are closely related to near-surface microstructural changes and residual stress. Thanks to the high spatial resolution residual stress analysis by synchrotron X-ray diffraction (SXRD) and neutron diffraction (ND) we could demonstrate that localized SF sources without any obvious microstructural variations are associated with steep stress gradients. The higher spatial resolution in SXRD stress characterization provides a good correlation between both GMR-SF and residual stress values and profiles (especially the location of the maxima). Such correlation is better than that between ND and GMR-SF measurements, because SXRD probes similar (shallow) depth as GMR-SF, while ND probes the bulk of a specimen. The excellent correlation between GMR-SF and SXRD is especially visible considering regions outside the heat affected zone (HAZ), where the influence of microstructural feature inside weld/HAZ is less pronounced and steep residual stress profiles are present.

Acknowledgements Authors would like to thank the colleagues from BAM N. Sonntag, B. Skrotzki, M. Marten, A. Böcker, A. Pittner, T. Michael, from Helmholtz Zentrum Berlin M. Boin, R. Wimpory, M. Klaus and Ch. Genzel, and from the University Stuttgart M. Kreutzbruck for their support to our work.

Funding Open Access funding enabled and organized by Projekt DEAL.

Declarations

Conflict of interests The authors declare that they have no potential conflicts of interest regarding this research.

Open Access This article is licensed under a Creative Commons Attribution 4.0 International License, which permits use, sharing, adaptation, distribution and reproduction in any medium or format, as long as you give appropriate credit to the original author(s) and the source, provide a link to the Creative Commons licence, and indicate if changes were made. The images or other third party material in this article are included in the article's Creative Commons licence, unless indicated otherwise in a credit line to the material. If material is not included in



the article's Creative Commons licence and your intended use is not permitted by statutory regulation or exceeds the permitted use, you will need to obtain permission directly from the copyright holder. To view a copy of this licence, visit <http://creativecommons.org/licenses/by/4.0/>.

References

- Bozorth RM (2003) *Ferromagnetism*. (Wiley-IEEE Press, Hoboken, USA, 2003) 992
- Kneller E, Seeger A, Kronmüller H (1962) *Ferromagnetismus*. Springer, Berlin Heidelberg
- Coey JMD (2010) *Magnetism and Magnetic Materials*. (Cambridge University Press 2010)
- Schneider CS (2005) Effect of stress on the shape of ferromagnetic hysteresis loops. *J Appl Phys* 97
- Cullity BD (1971) *JOM* 23:35–41
- Cullity BD, Graham CD (2009) *Introduction to Magnetic Materials*. (Wiley-IEEE Press, Hoboken, NJ, USA, 2009)
- Sablik MJ, Riley LA, Burkhardt GL, Kwun H, Cannell PY, Watts KT, Langman RA (1994) Micromagnetic model for biaxial stress effects on magnetic properties. *J Magn Magn Mater* 132:131–148
- Buttle DJ, Dalzell W, Scruby CB, Langman RA (1990) Comparison of three magnetic techniques for biaxial stress measurement. In: Thompson DO, Chimenti DE (eds) *Review of progress in quantitative nondestructive evaluation*. Springer, Boston, MA, pp 1879–1885
- Langman R (1990) *IEEE Trans Magn* 26:1246–1251
- Langman R (1982) *NDT Int* 15:91–97
- Schneider CS, Richardson JM (1982) *J Appl Phys* 53:8136–8138
- Sablik MJ (1995) *Nondestructive Testing and Evaluation* 12:87–102
- Schneider CS (2001) In *Trends in Materials Science Research*, ed. B. M. Caruta (Nova Science Publishers: 2006). 1–48
- DIN EN ISO 9934-1:2002-03 (2001) *Zerstörungsfreie Prüfung - Magnepulverprüfung- Teil 1: Allgemeine Grundlagen* (german)
- DIN 54136 (1988) *Magnetische Streuflussprüfung mit Sondenabtaugung* (withdrawn) (german)
- Foerster F (1981) *Materialpruefung* 23:372–378
- Förster F (1985) *Mater Eval* 43:1398–1404
- Förster F (1985) *Mater Eval* 43:1154–1162
- Förster F (1986) *NDT Int* 19:3–14
- Aharoni A (2001) *Introduction to the Theory of Ferromagnetism*, 2nd edn. Oxford University Press, Oxford
- Pelkner M, Neubauer A, Reimund V, Kreutzbruck M, Schütze A (2012) *Sensors* 12
- Pelkner M (2014) *Untersuchung und Anwendung von GMR-Sensorarrays für die Zerstörungsfreie Prüfung von ferromagnetischen Bauteilen*. Dissertation, Universität des Saarlandes
- Pelkner M, Stegemann R, Sonntag N, Pohl R, Kreutzbruck M (2018) Benefits of GMR sensors for high spatial resolution NDT applications. *AIP Conf Proc* 1949:040001
- Hubert A, Schäfer R (1998) *Magnetic Domains*. Springer, Berlin Heidelberg
- Nethi V, Ramalingeswara Rao V, Mamidi N, Kumar AG (2018) A critical review on residual stresses in welded joints. *Int J Scientific Res Development* 6:88–93
- Nasir NS, Razab MK, Ahmad MI, Mamat S (2016) Review on welding residual stress. *ARPN J Eng Appl Sci* 6166–6175
- Nitschke-Pagel T, Wohlfahrt H (2002) *Mater Sci Forum* 404–407:215–226
- Lim Y-S, Kim S-H, Lee K-J (2018) *Adv Mater Sci Eng* 2018:1–8
- Bruno G (2002) *Zeitschrift Fur Metallkunde* 93:33–41
- Bruno G, Dunn BD (2004) *J Pressure Vessel Technol* 126:284–292
- James MN, Webster PJ, Hughes DJ, Chen Z, Ratel N, Ting SP, Bruno G, Steuwer A (2006) *Mater Sci Eng, A* 427:16–26
- Stegemann R, Cabeza S, Lyamkin V, Bruno G, Pittner A, Wimpory R, Boin M, Kreutzbruck M (2017) *J Magn Magn Mater* 426:580–587
- Stegemann R, Cabeza S, Pelkner M, Lyamkin V, Pittner A, Werner D, Wimpory R, Boin M, Kreutzbruck M, Bruno G (2018) Influence of the microstructure on magnetic stray fields of low-carbon steel welds. *J Nondestruct Eval* 37
- Ch Genzel IA, Denks J, Gibmeier MK, Wagener G (2007) *Nuclear Instruments and Methods in Physics Research Section A: Accelerators. Spectrometers, Detectors and Associated Equipment* 578:23–33
- Meixner M, Klaus M, Genzel Ch (2013) *J Appl Crystallogr* 46:610–618
- Spieß L, Teichert G, Schwarzer R, Behnken H, Genzel C (2009) *Moderne Röntgenbeugung* (german). Vieweg+Teubner, Wiesbaden. 564
- Hauk V (1997) *In Structural and Residual Stress Analysis by Non-destructive Methods*. Elsevier Science B.V, Amsterdam
- Kröner E (1958) *Z Phys* 151:504–518
- Thiede T, Cabeza S, Mishurova T, Nadammal N, Kromm A, Bode J, Haberland C, Bruno G (2018) Residual stress in selective laser melted Inconel 718: Influence of the removal from base plate and deposition hatch length. *Mater Perform Charact* 4:717–735
- Farajian M, Nitschke-Pagel T, Wimpory RC, Hofmann M, Klaus M (2011) *Materialwissenschaft und Werkstofftechnik*. 42:996–1001
- Bruno G (2007) *Int J Mater Res* 98:7279
- Vakili-Tahami F, Hayhurst DR (2007) *Phil Mag* 87:4383–4419
- Moturu SR (2015) PhD Thesis “Characterization of Residual Stress and Plastic Strain in Austenitic Stainless Steel 316L(N) Weldments”. Dissertation, The Open University, UK. 311

Publisher's Note Springer Nature remains neutral with regard to jurisdictional claims in published maps and institutional affiliations.

